Inorganic Chemistry

Article

pubs.acs.org/IC

Controlling Ground and Excited State Properties through Ligand Changes in Ruthenium Polypyridyl Complexes

Dennis L. Ashford, Christopher R. K. Glasson, Michael R. Norris, Javier J. Concepcion, Shahar Keinan, M. Kyle Brennaman, Joseph L. Templeton, and Thomas J. Meyer*

Department of Chemistry, University of North Carolina at Chapel Hill, CB 3290, Chapel Hill, North Carolina 27599, United States

Supporting Information

ABSTRACT: The capture and storage of solar energy requires chromophores that absorb light throughout the solar spectrum. We report here the synthesis, characterization, electrochemical, and photophysical properties of a series of Ru(II) polypyridyl complexes of the type $[Ru(bpy)_2(N{-}N)]^{2+}$ (bpy = 2,2′-bipyridine; N−N is a bidentate polypyridyl ligand). In this series, the nature of the N−N ligand was altered, either through increased conjugation or incorporation of noncoordinating heteroatoms, as a way to use ligand electronic properties to tune redox potentials, absorption spectra, emission spectra, and excited state energies and lifetimes. Electrochemical measurements show that lowering the π^* orbitals on the N−N ligand results in more positive $Ru^{3+/2+}$ redox potentials and more positive first ligand-based reduction potentials. The metal-to-ligand charge transfer absorptions of all of the new complexes are mostly red-shifted compared to $Ru(bpy)_3^{2+}$ (λ_{max} = 449 nm) with the lowest energy MLCT absorption appearing at λ_{max} = 564 nm. Emission energies decrease from λ_{max} = 650 nm to 885 nm across the series. One-mode Franck−Condon analysis of room-temperature emission spectra are used to calculate key excited state properties, including excited state redox potentials. The impacts of ligand changes on visible light absorption, excited state reduction potentials, and $Ru^{3+/2+}$ potentials are assessed in the context of preparing low energy light absorbers for application in dye-sensitized photoelectrosynthesis cells.

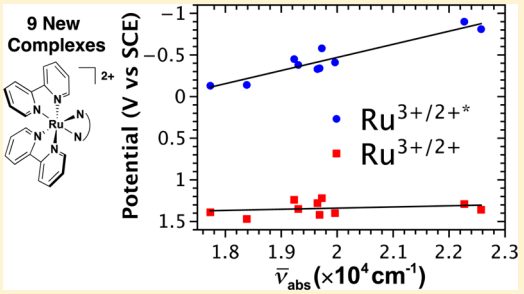

INTRODUCTION

Utilization of solar energy to produce fuels requires the integration of UV−vis−NIR light absorption with a sequence of electron and proton transfer events to drive water splitting ($2H_2O \rightarrow 2H_2 + O_2$) or water reduction of CO_2 to carbon-based fuels.[1−5] Honda and Fujishima demonstrated light driven water splitting by direct band gap excitation of TiO_2 (~3.2 eV) where the photogenerated holes (h^+) carry out water oxidation.[6] However, the high energy photons (<390 nm) required for direct band gap excitation of TiO_2 make up <10% of the available solar spectrum. The energy threshold for water splitting at 1.23 eV/eq requires 4 photons at 1000 nm at zero overpotential, with the energy of the optical transition a good measure of the free energy content of absorbed photons.[7−13]

One approach to solar fuels and artificial photosynthesis is the use of dye-sensitized photoelectrosynthesis cells (DSPECs).[14−16] They utilize chromophore-catalyst assemblies, for light absorption and catalysis, surface-bound to high band gap oxide semiconductors, notably TiO_2, for photoanode applications. In a DSPEC, excitation and injection by the chromophore initiates a sequence of events leading to oxidative activation of the catalyst.

For applications in water splitting at a photoanode, desirable properties of the chromophore include absorbing low energy/near-IR light and using electron injection into TiO_2 to create a surface-bound oxidant sufficiently powerful to drive water oxidation.[4,14,17−19] These ligand-influenced properties are counterbalanced by the need for excitation to produce an excited state sufficiently reducing to undergo efficient electron injection into low-lying conduction band states in TiO_2 with a conduction band edge at pH 0 of ~ −0.34 V versus SCE.[16,20,21] Other metal oxides, such as SnO_2[22,23] (E_{CB} ~ −0.04 V vs SCE in pH 0) and WO_3[24,25] (E_{CB} ~ 0.06 V vs SCE in pH 0), with more positive conduction band edges, resulting in increased driving force for electron injection from an excited state, have also been investigated.

Ruthenium polypyridyl complexes have found extensive use as chromophores in dye-sensitized solar cells (DSSCs) and DSPECs.[1,16,26−32] The properties of their low-lying metal-to-ligand charge transfer (MLCT) excited states are well understood, and they can be surface-bound to oxide surfaces, including TiO_2, as carboxylate or phosphonate derivatives.[33−35] Following MLCT excitation and electron injection, the oxidized forms of the complexes are typically powerful oxidants with redox potentials sufficient to drive water oxidation catalysis. Both excited state energy and redox potentials can be varied systematically by ligand modifications.[36−42]

We have reported the preparation and characterization of a series of ruthenium based chromophore-catalyst assemblies for

Received: February 19, 2014
Published: May 21, 2014

   dx.doi.org/10.1021/ic500408j | Inorg. Chem. 2014, 53, 5637−5646

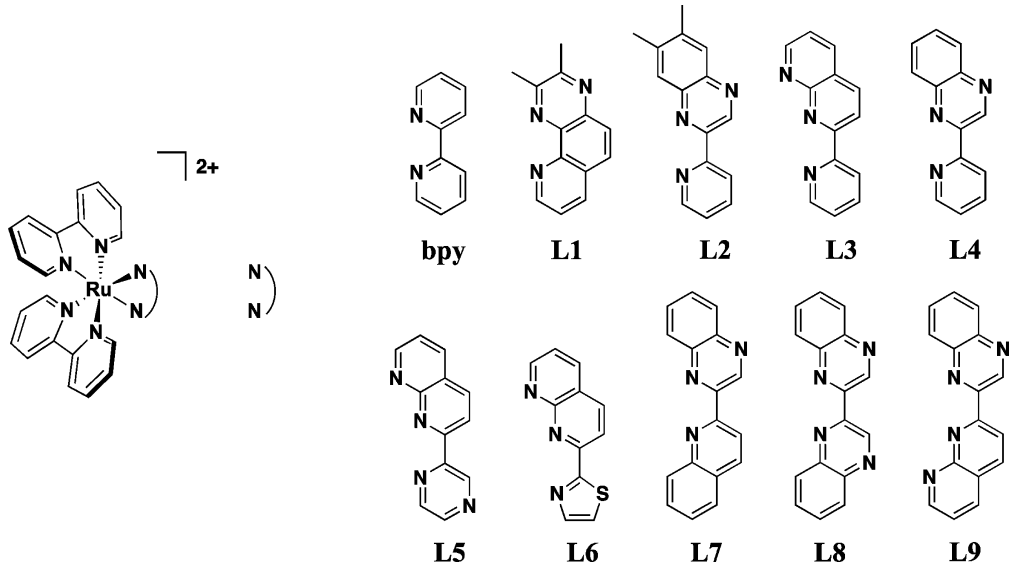

Figure 1. Structures of the generic complex and ligands in the series $[Ru(bpy)_2(N{-}N)]^{2+}$.

use in DSPEC devices based on derivatized forms of $Ru(bpy)_3^{2+}$ (bpy = 2,2′-bipyridine) as the light harvesting chromophore.[43−50] We report here the preparation and properties of a series of heteroleptic Ru(II) polypyridyl chromophores having the general structure $[Ru(bpy)_2(N{-}N)]^{2+}$ (N−N is a bidentate polypyridyl ligand). The series was designed to explore the manipulation of light absorption from the visible into the near-IR while retaining both the ground state oxidation potentials necessary for water oxidation and sufficient excited state redox potentials for electron injection into the semiconductor conduction band. The library of complexes synthesized in this work is represented in Figure 1.

RESULTS AND DISCUSSION

Ligand Synthesis. To tune the redox and photophysical properties of the ruthenium complexes, the π^* acceptor levels of the N−N ligands (**L1**−**L9**) were systematically altered. This was accomplished by using two different ligand designs: (1) incorporation of noncoordinating heteroatoms and (2) introduction of extended conjugation in the ligand backbone through fused aromatic rings. To achieve these structural features, pyrazine, thiazole, quinoxaline, quinoline, and naphthyridine moieties in various combinations were introduced into the diimine ligand (N−N), Figure 1.

L1 was prepared in high yield by the condensation of 7,8-diaminequinoline and 2,3-butadione in ethanol (Scheme 1). 7,8-Diaminequinoline was prepared in four steps starting from 1,2,3,4-tetrahydroquinoline. First, 1,2,3,4-tetrahydroquinoline was converted to 7-nitro-1,2,3,4-tetrahydroquinoline in a mixed acid electrophilic aromatic substitution.[51] The nitrated hydroquinoline was then oxidized with 2,3-dichloro-5,6-dicyano-1,4-benzoquinone (DDQ) to give 7-nitroquinoline.[52] This latter product was converted into 7-nitroquinoline-8-amine by treatment with hydroxylamine hydrochloride under basic conditions followed by reduction of the nitro group with Raney nickel to give 7,8-diaminequinoline (Scheme 1).[53]

The *p*-quinoxaline pyridine ligands **L2** and **L4** were prepared in 45% and 85% yield, respectively, by a reported acid catalyzed condensation of *o*-phenylenediamine precursors with 2-acetylpyridine (Scheme 2).[54]

Scheme 1. Synthesis of L1

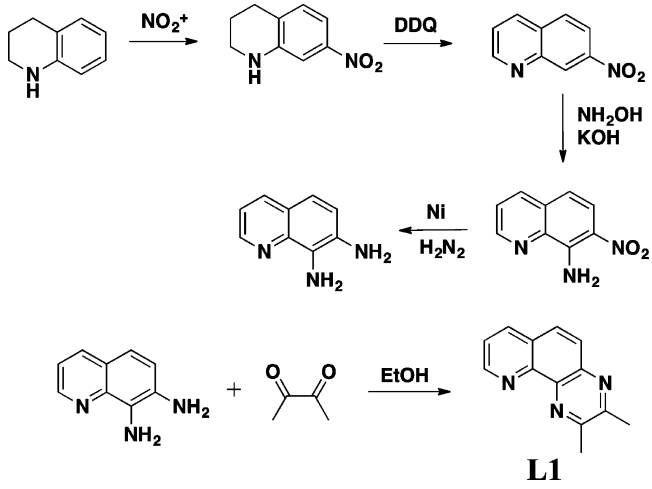

Scheme 2. Synthesis of *p*-Quinoxaline Pyridine Ligands L2 and L4

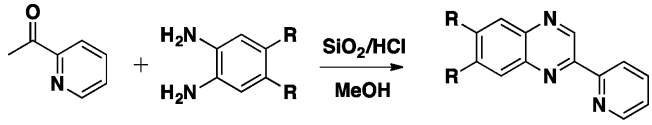

L2, R = H
L4, R = Me

The Friedländer condensation was used to prepare a series of quinoline (**L7**) and naphthyridine (**L3**, **L5**, **L6**, **L9**) derivatives with heterocyclic substituents in the 2-position (Scheme 3). These substituents include pyridine (**L3**), pyrazine (**L5**), thiazole (**L6**), quinoline (**L7**), and quinoxaline (**L9**).[55] This synthetic approach allows for access to a library of subtly varied ligands for systematic studies. **L8** was synthesized by a reported procedure.[56] See Supporting Information for the full experimental procedure for the syntheses of **L1**−**L9**.

Complex Syntheses. The $[Ru(bpy)_2(N{-}N)]^{2+}$ complexes were isolated as their chloride salt (or by salt metathesis, to

dx.doi.org/10.1021/ic500408j | Inorg. Chem. 2014, 53, 5637−5646

Scheme 3. General Synthetic Route for Ligand Synthesis via Friedländer Condensations

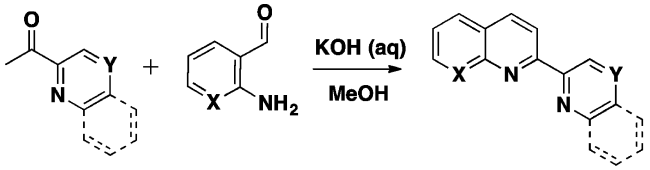

L3, X = N, Y = C
L5, X = N, Y = N
L7, X = C, Y = N
L9, X = N, Y = N

form perchlorate or hexafluorophosphate salts) by the reaction of $Ru(bpy)_2Cl_2$[57] with each of the bidentate (N−N) ligands **L1**−**L9** in 1:1 $EtOH/H_2O$ (see Supporting Information). In general, these reactions can be followed by UV−vis absorption spectral measurements by monitoring disappearance of the $Ru(bpy)_2Cl_2$ MLCT absorptions (λ_{max} = 363 and 526 nm in CH_3CN)[58] and the appearance of absorptions due to complexes **1**−**9** (Table 1, Supporting Information).

Single crystal X-ray analysis was performed on complex **6** (Figure 2) to ensure the sulfur in **L6** did not coordinate

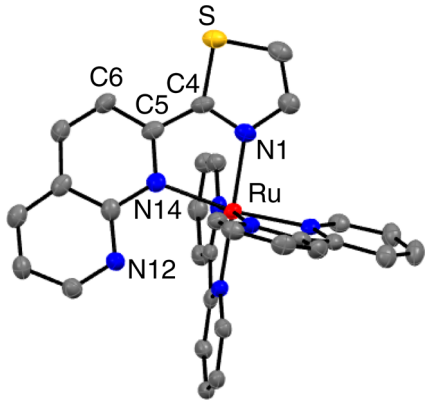

Figure 2. ORTEP diagram of complex **6** from single crystal X-ray analysis with thermal ellipsoids at the 50% probability level. Hydrogen atoms are omitted for clarity.

Table 1. Spectroscopic Properties and Redox Potentials for the Series 1−9, Figure 1

		emission at RT[b]						
complex	absorbance λ (nm) (ε, $\times 10^4$ M^{-1} cm^{-1})[a]	λ_{max} (nm)	τ (ns)	ΔG_{ES}[c] (eV)	$E_{1/2}$ ($Ru^{3+/2+}$) V[d]	$E_{1/2}$ ($Ru^{3+/2+*}$) V[e]	$E_{1/2}$ ($Ru^{2+*/+}$) V[f]	$E_{1/2}$ ($Ru^{2+/+}$) V[d]
$Ru(bpy)_3^{2+}$	449 (1.4) 286 (5.1) 243 (2.5)	620	831	2.19	1.29	−0.90	0.89	−1.30
1	443 (1.3) 285 (5.4) 249 (1.9)	650	26	2.17	1.36	−0.81	1.05	−1.12
2	501 (0.63) 283 (4.5) 254 (2.1)	755	167	1.81	1.40	−0.41	0.98	−0.83
3	507 (0.77) 287 (5.1) 244 (3.4)	765	184	1.80	1.22	−0.58	0.84	−0.96
4	508 (0.90) 281 (5.4) 254 (3.0)	780	105	1.76	1.42	−0.34	1.02	−0.74
5	518 (0.77) 284 (4.8) 242 (3.2)	790	92	1.73	1.35	−0.38	0.95	−0.78
6	520 (0.81) 286 (4.6) 249 (2.2)	810	113	1.69	1.24	−0.45	0.80	−0.89
7	544 (0.81) 286 (4.7) 256 (3.1)	830	93	1.61	1.47	−0.14	1.00	−0.61
8	509 (0.66) 288 (3.6) 253 (3.2)	850	30	1.61	1.28	−0.33	0.71	−0.57
9	564 (0.75) 285 (4.2) 254 (3.4)	885	26	1.52	1.39	−0.13	0.96	−0.56

[a] In CH_3CN. [b] In CH_3CN deaerated with Ar for 30 min. [c] ΔG_{ES} from a Franck−Condon analysis of emission spectra in CH_3CN, see text. [d] In CH_3CN deaerated with Ar for 10 min, 1 mM in complex and 0.1 M $TBAPF_6$ supporting electrolyte. GC working electrode, Pt-wire counter electrode, and $Ag/AgNO_3$ (1 M) reference (values were adjusted to agree with literature values for $[Ru(bpy)_3]^{3+/2+}$ at 1.29 V vs SCE).[37−39,58] $E_{1/2}$ values from differential pulse voltammetry. [e] $Ru^{3+/2+*} = Ru^{3+/2+} - \Delta G_{ES}$. [f] $Ru^{2+*/+} = Ru^{2+/+} + \Delta G_{ES}$.

dx.doi.org/10.1021/ic500408j | Inorg. Chem. 2014, 53, 5637−5646

competitively with the nitrogen. As shown in Figure 2, the nitrogen is coordinated to the Ru center and has a slightly distorted octahedral geometry around the Ru center (N1−Ru−*N* = 173.7°, N14−Ru−*N* = 170.0°). Steric repulsions between N12 and one of the bipyridine ligands distort the planarity of **L6** upon coordination to the Ru center as indicated by the S−C4−C5−C6 torsion angle of 8.7°. The length of the Ru−N1 bond (2.056 Å) is similar to that of the Ru−pyridine nitrogen distance, whereas the Ru−N14 (2.122 Å) is slightly elongated due to the steric repulsion between N12 and the bipyridine ligand.[59] The DFT computed geometry of complex **6** shows the same trends, with distorted octahedral geometry around the Ru center (N1−Ru−*N* = 175.2°, N14−Ru−*N* = 170.6°) and the Ru−N1 bond (2.074 Å) shorter than that of Ru−N14 (2.178 Å), Supporting Information Figure S13.

Electrochemistry. The electrochemical properties of complexes **1**−**9** in dry CH_3CN (0.1 M $TBAPF_6$ supporting electrolyte, TBA = tetrabutylammonium) were examined by cyclic and square-wave voltammetry. $E_{1/2}$ values for the $Ru^{3+/2+}$ couple of each complex, eq 1, are reported in Table 1 with representative cyclic voltammograms shown in Figure 3. All complexes exhibit reversible $Ru^{3+/2+}$ redox couples with $E_{1/2}$ values ranging from 1.22 to 1.47 V (vs SCE).

$$[Ru^{III}(bpy)_2(N{-}N)]^{3+} \xrightarrow{+e^-} [Ru^{II}(bpy)_2(N{-}N)]^{2+} \quad (1)$$

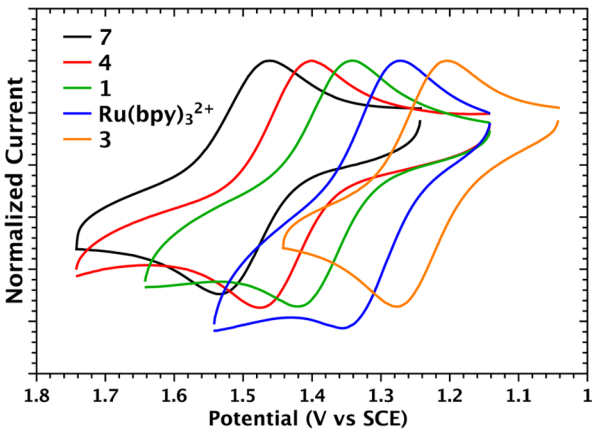

Figure 3. Cyclic voltammogram at 100 mV/s of complexes **7** (black), **4** (red), **1** (green), $Ru(bpy)_3^{2+}$ (blue), and **3** (orange) in dry CH_3CN at 22 °C with a glassy carbon working electrode, Pt-wire counter electrode, and a $Ag/AgNO_3$ reference electrode with $E_{1/2}(Ru(bpy)_3^{3+/2+})$ = 1.29 V vs SCE.

In general, the complexes that incorporate pyrazine units (**2**, **4**, **5**, **7**, **8**, **9**) have $Ru^{3+/2+}$ redox potentials that are more positive than the $[Ru(bpy)_3]^{3+/2+}$ couple (1.29 V vs SCE).[39−41,60] All of the ligands (**L1**−**L9**) have lower-lying π^* orbitals compared to bpy. The decrease in the N−N π^* orbital energy increases $d\pi-\pi^*$ back bonding from the Ru^{II} center to the N−N ligand, stabilizing the $d\pi^6$ electronic configuration, resulting in increased redox potentials for the $Ru^{3+/2+}$ couples.[60−62] Complex **8** is a special case in that it has a relatively low $Ru^{3+/2+}$ redox potential (1.28 V vs SCE) considering the electronic nature of **L8** with two pyrazine groups in the ligand framework. Molecular models of **8** indicate that **L8**, when bound to the Ru^{II} center, is significantly distorted from planarity (Supporting Information Figure S12). This could result in a disruption in the aromaticity in the ligand raising the π^* energy levels, causing a lower than expected $Ru^{3+/2+}$ potential. Attempts to grow X-ray quality crystals of **8** were unsuccessful.

The first ligand-based reduction potentials ($Ru^{2+/+}$, eq 2) in dry CH_3CN (0.1 M $TBAPF_6$ supporting electrolyte) are listed in Table 1.[41] The variations in the first reduction potential ($Ru^{2+/+}$), −1.12 V to −0.56 V, are significantly larger than variations in the $Ru^{3+/2+}$ potentials, consistent with reduction at **L1**−**L9** as acceptor ligands. The 0.56 V variance in ligand-based reduction potentials reflects the effect of increased conjugation and/or incorporation of heteroatoms on the π^* acceptor levels in the acceptor ligands.[60] As shown in Figure 4 for $Ru(bpy)_3^{2+}$

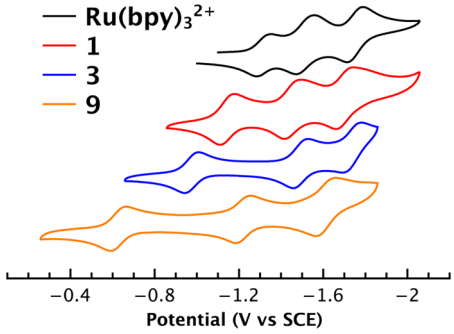

Figure 4. Cyclic voltammogram at 100 mV/s for complexes **9** (orange), **3** (blue), **1** (red), and $Ru(bpy)_3^{2+}$ (black), in dry CH_3CN at 22 °C under a nitrogen atmosphere with a glassy carbon working electrode, Pt-wire counter, and a $Ag/AgNO_3$ reference (relative to $Ru(bpy)_3^{3+/2+}$ at 1.29 V vs SCE).

and complexes **1**, **3**, and **7**, three reversible ligand-based reduction waves appear from −0.20 V to −2.0 V (vs SCE) with the first ligand-based reduction ranging from −0.56 V to −1.12 V (vs SCE).

$$[Ru^{II}(bpy)_2(N{-}N)]^{2+} \xrightarrow{+e^-} [Ru^{II}(bpy)_2(N{-}N^{\bullet-})]^{+} \quad (2)$$

Complex **3** has a lower $Ru^{3+/2+}$ potential than $Ru(bpy)_3^{2+}$ by 70 mV (Table 1), suggesting that **L3** is a worse π^*-acceptor ligand than bpy even though its first ligand-based reduction (−0.96 V vs SCE) is 340 mV less negative than reduction of $Ru(bpy)_3^{2+}$ (−1.30 V vs SCE).[41,63] This is an apparent consequence of decreased orbital mixing with $d\pi(Ru^{II})$ highlighting the roles of both ligand π^* acceptor energy and orbital mixing in the design of acceptor ligands.

UV−Vis Absorption. UV−vis spectra of complexes **1**−**9** in acetonitrile all feature characteristic, intense $\pi \rightarrow \pi^*$ absorptions below 350 nm ($\varepsilon \approx 3.5{-}5.5 \times 10^4$ M^{-1} cm^{-1}) along with metal-to-ligand charge transfer (MLCT) absorptions (Table 1) in the visible region. All MLCT absorptions observed experimentally are from singlet ground states to ^{1}MLCT excited states. For complexes of Ru^{II}, the corresponding ground state to ^{3}MLCT absorptions have low oscillator strengths and are difficult to observe.[64,65] The most notable trend in the series is the red shift in the lowest energy MLCT absorption from λ_{max} = 443 nm (**1**) to λ_{max} = 564 nm (**9**) with molar extinction coefficients that range from $\varepsilon = 6.3 \times 10^3$ M^{-1} cm^{-1} (**2**) to $\varepsilon = 1.3 \times 10^4$ M^{-1} cm^{-1} (**1**). Representative spectra are shown in Figure 5, and the remaining spectra are available in Supporting Information.

The energies of the lowest energy MLCT absorptions are influenced by both increased conjugation in the N−N ligand and the presence of noncoordinating heteroatoms. The

dx.doi.org/10.1021/ic500408j | Inorg. Chem. 2014, 53, 5637−5646

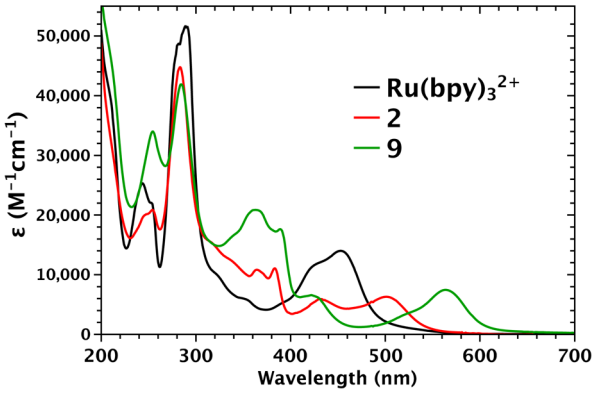

Figure 5. UV−vis spectra of $Ru(bpy)_3^{2+}$, **2**, and **9** in CH_3CN.

absorption spectra of complexes **2** and **9** illustrate a splitting in the MLCT manifolds. They arise from transitions to both bpy and the N−N ligands and, at higher energies, to higher lying π^* acceptor orbitals on the N−N ligands (Figure 5). The lowest energy transitions to bpy and N−N are illustrated in eqs 3 and 4. The extent of MLCT splitting between bpy and N−N as acceptor ligands increases with the π^* acceptor ability of N−N.[36,38,66] The use of multiple π^* acceptor ligands to access transitions to higher π^* levels was utilized in earlier studies that focused on creating "black" MLCT absorbers.[36]

$$[Ru^{II}(bpy)_2(N{-}N)]^{2+} \xrightarrow{h\nu} [Ru^{III}(bpy^{\bullet-})(bpy)(N{-}N)]^{2+*} \quad (3)$$

$$[Ru^{II}(bpy)_2(N{-}N)]^{2+} \xrightarrow{h\nu} [Ru^{III}(bpy)_2(N{-}N^{\bullet-})]^{2+*} \quad (4)$$

To better understand the absorption spectra, we calculated the electronic spectra of complexes **1**−**9**. The DFT optimized geometries (using the B3LYP/LanL2DZ functional/basis-set) were analyzed by TD-DFT calculations (using the PBE0/LanL2DZ functional/basis-set, Supporting Information Figure S14). A continuum model was used for the solvent. The results of the calculations are summarized in Table 2 and Supporting Information Figure S14. The computed spectra correlate well with experimental spectra with strong $\pi \rightarrow \pi^*$ absorptions predicted below 300 nm and MLCT absorptions at longer wavelengths. The calculations also verify the origins of the intense visible absorptions from 400−600 nm (MLCT transitions) as excitations from Ru^{II} either to bpy (eq 3) or to the N−N ligand for **L1**−**L9** (eq 4). All computed spectra are blue-shifted relative to the experimental spectra, likely due to the inherent TD-DFT overestimation of MLCT energies in Ru polypyridyl complexes as well as solvent effects that are not adequately described by the polarizable continuum model (PCM) model used here.[67]

Table 2 compares band assignments from the DFT calculations for complexes **2** and **9**. For complex **2**, the spectra are dominated in the UV by a bpy ligand-based $\pi \rightarrow \pi^*$ transition at ∼270 nm and high energy MLCT transitions from the $d\pi$ orbital on Ru^{II} to π^* on bpy at 308 nm, and multiple transitions from the $d\pi$ orbital on Ru^{II} to π^* on bpy and N−N ligand at 408 and 475 nm. Calculated orbital compositions are shown in Supporting Information Figure S15 for the $d\pi(Ru^{II}) \rightarrow \pi^*(N{-}N)$ transition in complex **2**. For complex **9**, the calculations point to the band at 278 nm as an overlap between $\pi \rightarrow \pi^*$ transitions for the bpy and N−N ligands. The band at ∼326 nm arises from MLCT transitions between $d\pi(Ru) \rightarrow \pi_2^*(N{-}N)$ and $d\pi(Ru) \rightarrow \pi^*(bpy)$. The two low energy bands at 425 and 758 nm both arise from MLCT from the HOMO (mixed $d\pi(Ru) + \pi(N{-}N)$) to π^* on the N−N ligand. The calculated transition at ∼758 nm for **9** has an absorptivity too low to observe experimentally.

Figure 6 shows calculated and experimental spectra for complex **2** in CH_3CN with the calculated transition energies

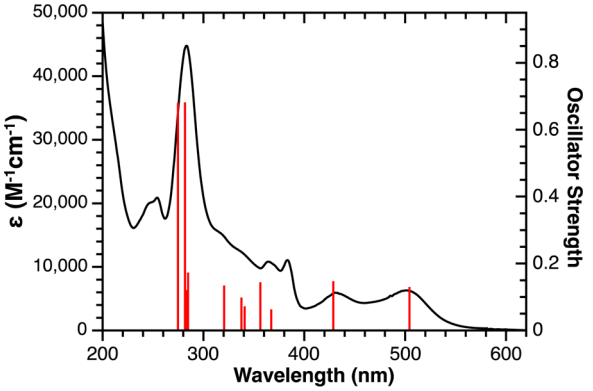

Figure 6. UV−vis spectrum of complex **2** at room temperature in CH_3CN (black line) and calculated TD-DFT transitions (vertical red bars with heights illustrating oscillator strengths, red-shifted by 0.15 eV).

shown as vertical bars with their heights reflecting relative oscillator strengths. To help in visualization, the calculated transitions are red-shifted by 0.15 eV. Both the observed and calculated spectra illustrate the ∼75 nm split in absorption

Table 2. Comparison of TD-DFT Calculated Absorption Maxima for Complexes 2 and 9 in CH_3CN

complex **2**			complex **9**		
exptl (ε, × 10^4 M^{-1} cm^{-1})	calcd	transition	exptl (ε, × 10^4 M^{-1} cm^{-1})	calcd	transition
254 nm (2.1)	266 nm	$\pi(N{-}N) \rightarrow \pi^*(N{-}N)$	254 nm (3.4)	278 nm	$\pi(N{-}N) \rightarrow \pi^*(bpy)$
	272 nm	$\pi(bpy) \rightarrow \pi^*(bpy)$			
	274 nm	$\pi(bpy) \rightarrow \pi^*(bpy)$			
	275 nm	$\pi(bpy) \rightarrow \pi^*(bpy)$			
283 nm (4.5)	308 nm	$d\pi(Ru) \rightarrow \pi^*(bpy)$	285 nm (4.2)	325 nm	$d\pi(Ru) \rightarrow \pi^*(N{-}N)$
	342 nm	$\pi(N{-}N) \rightarrow \pi^*(N{-}N)$		326 nm	$d\pi(Ru) \rightarrow \pi^*(N{-}N)$
				355 nm	$d\pi(Ru) \rightarrow \pi^*(N{-}N)$
501 nm (0.6)	408 nm	$d\pi(Ru) \rightarrow \pi^*(bpy)$	425 nm (0.66)	428 nm	$d\pi(Ru) + \pi(N{-}N) \rightarrow \pi^*(N{-}N)$
	475 nm	$d\pi(Ru) \rightarrow \pi^*(N{-}N)$			
			564 nm (0.75)	758 nm	$d\pi(Ru) + \pi(N{-}N) \rightarrow \pi^*(N{-}N)$

dx.doi.org/10.1021/ic500408j | Inorg. Chem. 2014, 53, 5637−5646

maxima between the MLCT transitions to π^*(bpy) and π^*(N−N) shown in eqs 3 and 4.

Emission Spectra. Complexes **1**−**9** exhibit broad emission spectra at room temperature in CH_3CN with emission energies decreasing from **1** (λ_{max} = 650 nm, 1.54 × 10^4 cm^{-1}) to **9** (λ_{max} = 885 nm, 1.12 × 10^4 cm^{-1}) relative to emission from $Ru(bpy)_3^{2+*}$ at λ_{max} =620 nm (1.61 × 10^4 cm^{-1}). Emission spectra are compared to $Ru(bpy)_3^{2+*}$ in Figure 7 with emission

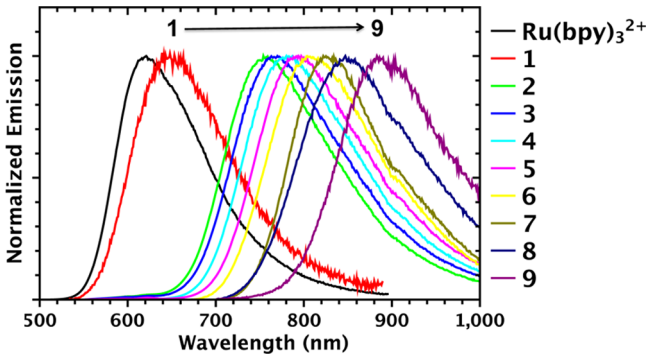

Figure 7. Normalized emission spectra for $Ru(bpy)_3^{2+}$ and **1**−**9** in argon deaerated acetonitrile at room temperature.

energies listed in Table 1. Emission from these complexes occurs from the lowest lying ^{3}MLCT excited states following intersystem crossing from the initial ^{1}MLCT excited states that dominate absorption.[42,65,68]

Trends in emission energies follow those for the lowest energy MLCT absorptions with the highest energy absorption and emission from **1** at $\lambda_{max,abs}$ = 443 nm (2.26 × 10^4 cm^{-1}) and $\lambda_{max,em}$ = 650 nm (1.54 × 10^4 cm^{-1}). Variations in acceptor ligand cause red shifts in the lowest MLCT absorption of >100 nm (4.8 × 10^3 cm^{-1}) for **9** compared to **1** and of >200 nm (4.2 × 10^3 cm^{-1}) for emission from **9** compared to **1**.

Time-resolved emission decay measurements were conducted by time-correlated single photon counting (TCSPC) following 444 nm excitation. Lifetimes (τ) for this class of chromophores are largely dictated by nonradiative decay with η_{em} = 6.2% and k_{nr} = 4.8 × 10^5 s^{-1} for $Ru(bpy)_3^{2+*}$ under these conditions, with $\tau^{-1} \sim k_{nr}$.[65] In addition to MLCT vibrational decay, k_{nr} also includes contributions from thermal population and subsequent rapid deactivation through a low-lying dd excited state pathway.[37,68−71]

As shown by the energy gap law plot of ln τ^{-1} versus emission energy in Figure 8, the decrease in lifetime with changes in acceptor ligand is qualitatively consistent with energy gap law behavior.[42] The existence of the linear correlation in Figure 8 suggests that contributions from nonradiative decay from the lowest, emitting MLCT state dominate with dd state participation being relatively unimportant. This is expected given the relatively low energies of the diazine-based (N−N) MLCT excited states.[42,72−74] Complex **1** is the outlier in the correlation, perhaps due to steric crowding. Distortions in the metal−ligand framework induce dσ^*−dπ orbital mixing, decreasing the energy of low-lying dd states and introducing an additional nonradiative decay pathway.[68,75−77]

Previous studies on related Os^{II} and Ru^{II} diimine complexes of the type $M^{II}(bpy)_2L_2^{2+}$ and $M^{II}(bpy)_2(L-L)^{2+}$ (M = Os or Ru) have shown that absorption and emission energies increase linearly with the electrochemical gap $\Delta E_{1/2}$, with $\Delta E_{1/2}$ being the difference between the ground state $Ru^{3+/2+}$ potential

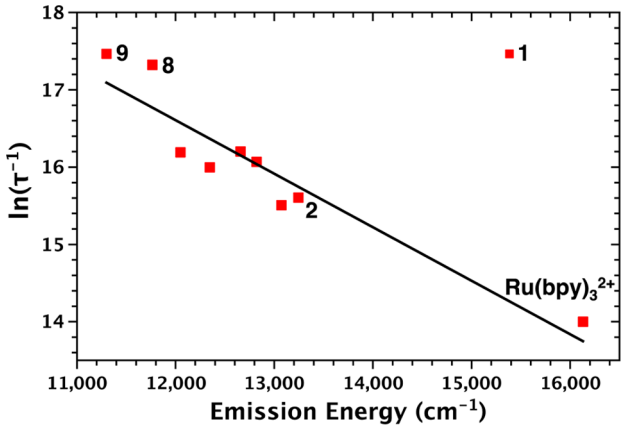

Figure 8. Plot of emission energy vs ln τ^{-1} for complexes **1**−**9** and $Ru(bpy)_3^{2+}$ in CH_3CN at 25 °C.

($E_{1/2}(Ru^{3+/2+})$) and the potential for the first ligand-based reduction ($E_{1/2}(Ru^{2+/+})$).[39,42,78,79] Figure 9 illustrates how the lowest energy absorption ($\bar{\nu}_{abs}$) and emission ($\bar{\nu}_{em}$) maxima vary with $\Delta E_{1/2}$ at room temperature. The linear relationship is expected for transitions to and emission from MLCT excited states.[42,78,80] It is also noteworthy that the slopes of 0.84 for absorption and 0.73 for emission are near 1 and are similar to each other.

Emission energies for complexes **1**−**9** also decrease linearly with $E_{1/2}(Ru^{2+/+})$, Figure 9, showing that variations in excited state energies are mainly a consequence of variations in the energy of the acceptor ligand π^* levels. There is no correlation between emission energy and the ground state metal centered $Ru^{3+/2+}$ potential ($E_{1/2}(Ru^{3+/2+})$, see Supporting Information Figure S16).[80]

Emission Spectral Fitting. Correlation of Excited State Properties. Emission spectra for all nine complexes were analyzed by use of a one-mode Franck−Condon analysis of room-temperature emission spectra (see Supporting Information).[33,65,81−85] In this analysis contributions from medium frequency υ(bpy) modes are treated as a single averaged mode with low frequency modes and the solvent being included in the band widths. Spectra were fit to a series of vibronic lines centered on the 0−0 component at energy E_0 and separated by a vibrational quantum spacing of $\hbar\omega_M$. Only transitions from the $\nu' = 0$ level in the excited state to level ν in the ground state are included in the summation. Comparisons between experimental and calculated emission spectra for each complex and for $Ru(bpy)_3^{2+*}$ are shown in Supporting Information Figure S1.

In the spectral fits, relative intensities of the vibronic lines are determined by the electron-vibrational coupling constant, S_M, which is related to the equilibrium displacement change, ΔQ_{eq}, by $1/2\Delta Q_{eq}^2$. As noted above, additional vibrational contributions from low frequency modes and the solvent are treated classically and included in the bandwidth at half height, $\Delta\bar{\nu}_{1/2}$, with $\Delta\bar{\nu}_{1/2}$ defined in eq 5. In eq 5, $\lambda_{0,L}$ is the sum of the solvent reorganization energy, λ_0, and reorganization energy from low frequency modes, λ_L. E_0 in eq 5 is the 0−0 energy gap, the energy of the excited state above the ground state with both states in their $\nu = 0$ vibrational levels.

Results of the spectral fitting analysis are summarized in Table 3. The free energy content of the excited state above the ground state, ΔG_{ES}, was calculated by using eq 5. In eq 5, k_B is the Boltzmann constant and T is the temperature (298 K). As

dx.doi.org/10.1021/ic500408j | Inorg. Chem. 2014, 53, 5637−5646

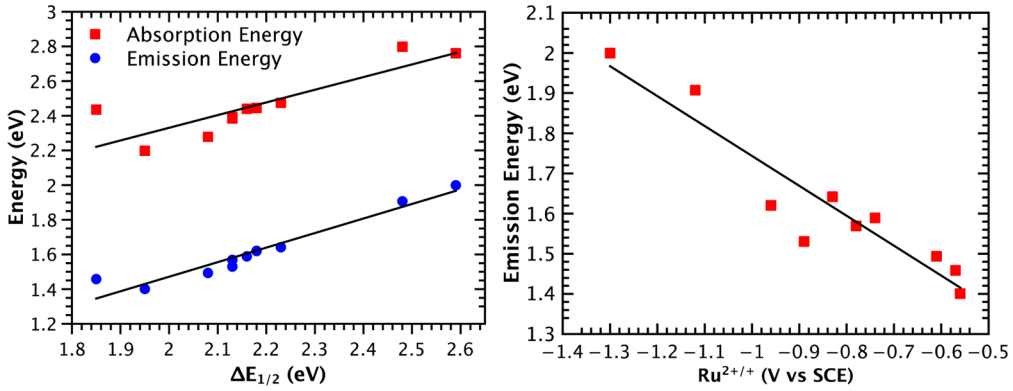

Figure 9. (Left) Variation of absorption, $\bar{\nu}_{abs}$, red squares, and emission, $\bar{\nu}_{em}$, blue circles, energies on the electrochemical gap ($\Delta E_{1/2} = E_{1/2}(Ru^{3+/2+}) - E_{1/2}(Ru^{2+/+})$ for $Ru(bpy)_3^{2+}$ and **1**–**9**. (Right) Variation of $\bar{\nu}_{em}$ with $E_{1/2}(Ru^{2+/+})$ in dry CH_3CN at 25 °C.

Table 3. Emission Spectral Fitting Parameters for MLCT Emission from $Ru(bpy)_3^{2+*}$ and 1–9 in MeCN at 25° C

complex	E_0 (cm^{-1})	$\Delta\bar{\nu}_{1/2}$ (cm^{-1})	$\hbar\omega_M$ (cm^{-1})	S_M	ΔG_{ES} (cm^{-1})
$Ru(bpy)_3^{2+}$	16 300	1800	1400	1.11	17 700
1	15 800	1950	1300	1.23	17 500
2	13 300	1750	1300	0.91	14 600
3	13 100	1790	1350	0.89	14 500
4	12 900	1700	1250	0.93	14 200
5	12 600	1750	1400	0.80	13 900
6	12 400	1700	1200	0.80	13 600
7	12 100	1450	1250	0.71	13 000
8	11 900	1581	1150	0.96	13 000
9	11 100	1583	1512	0.76	12 200

shown by the data in Table 1, variations in ΔG_{ES} mirror those in emission energy through the series with ΔG_{ES} decreasing from 2.18 eV for **1** to 1.57 eV for **9**.

$$\Delta G_{ES} = E_0 + \lambda_{0,L} = E_0 + \frac{(\Delta\nu_{1/2})^2}{16k_BT \ln 2} \quad (5)$$

Discerning systematic trends in the data in Table 3 is complicated by the fact that excited state properties are dictated largely by the acceptor ligand, which varies through the series. This can be seen in the relatively large range of $\hbar\omega_M$ values derived from the spectral fits. Nonetheless, one notable trend is the general decrease in electron-vibrational coupling constant (Huang–Rhys factor, S_M) as the energy gap decreases. This is consistent with a decrease in the extent of charge transfer as the energy gap decreases.[64,86,87] In addition, the increase in excited-state delocalization may also play a role in influencing the magnitude of S_M.[42,65,86] As expected, both the 0–0 energy gap (E_0) and the free energy content of the excited state above the ground state (ΔG_{ES}) decrease with the energy of the π^* acceptor level as measured by $E_{1/2}(Ru^{2+/+})$, Table 1.

Excited State Redox Potentials. Redox potentials for the MLCT excited states were calculated from ΔG_{ES} and the electrochemically measured ground state potentials by eqs 6 and 7.[28,37,80] Results for the series from **1** to **9** are summarized in Table 1.

$$E_{1/2}(Ru^{2+*/+}) = E_{1/2}(Ru^{2+/+}) + \Delta G_{ES} \quad (6)$$

$$E_{1/2}(Ru^{3+/2+*}) = E_{1/2}(Ru^{3+/2+}) - \Delta G_{ES} \quad (7)$$

A plot of ΔG_{ES} versus $E_{1/2}(Ru^{3+/2+*})$ is shown in Figure 10. Variations in the acceptor ligand decrease the reducing ability of the $[Ru^{III}(bpy)_2(N{-}N^{\bullet-})]^{2+*}$ excited state from −0.81 to

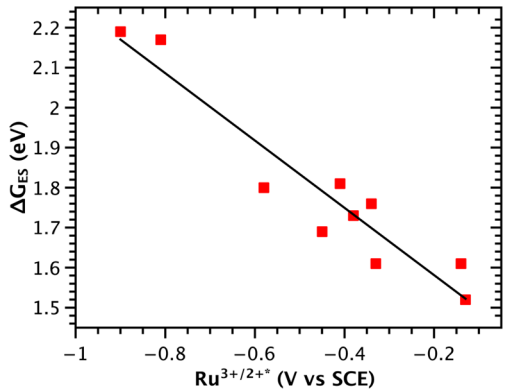

Figure 10. Dependence of the free energy content of the excited state (ΔG_{ES}) on $E_{1/2}(Ru^{3+/2+*})$.

−0.13 V (vs SCE) across the series from **1** to **9**.[80] As shown in Figure 11, ground state $Ru^{2+/+}$ ($d\pi^6/d\pi^6\pi^{*1}$) and excited state $Ru^{3+/2+*}$ ($d\pi^5/d\pi^5\pi^{*1}$) redox potentials, both ligand based, increase linearly with increasing emission energy. By contrast, ground state $Ru^{3+/2+}$ ($d\pi^5/d\pi^6$) and excited state $Ru^{2+*/+}$ ($d\pi^5\pi^{*1}/d\pi^6\pi^{*1}$) redox potentials, with the redox levels localized largely on the metal, remain relatively unchanged as the emission energy increases.

The relationship between the ligand-based $Ru^{2+/+}$ and $Ru^{3+/2+*}$ redox couples to the emission energy is an expected result given the ligand-based nature of the redox processes in eqs 2 and 8. This is in contrast to previously reported correlations based on complexes of the type $[M(bpy)_2(L)_2]^{2+}$ ($M = Os^{II}$, Ru^{II}) where the lowest π^* levels are based on bpy or phen (1,10-phenanthroline). In these series, the role of variations in L_2 is largely through the $d\pi(M^{II})$ donor levels

dx.doi.org/10.1021/ic500408j | Inorg. Chem. 2014, 53, 5637–5646

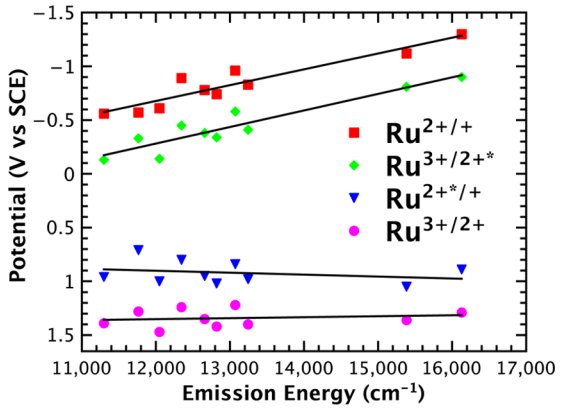

Figure 11. Variation of ground and excited redox potentials with emission energy in CH_3CN (0.1 M $TBAPF_6$ for electrochemical measurements) at 25 °C.

with $Ru^{3+/2+}$ and $Ru^{2+*/+}$ potentials increasing linearly with emission energy.[78,80,88−90] In the current series, with the lowest-lying acceptor levels on the N−N ligand, ground state $Ru^{3+/2+}$ and excited state $Ru^{2+/+*}$ potentials are relatively unchanged as the MLCT energy gap varies as shown in Figure 11.

$$[Ru^{III}(bpy)_2(N{-}N)]^{3+} \xrightarrow{+e^-} [Ru^{III}(bpy)_2(N{-}N^{\bullet-})]^{*2+} \quad (8)$$

Controlling Excited State Properties. The motivation for preparing and characterizing the series of complexes $[Ru^{II}(bpy)_2(N{-}N)]^{2+}$ was to explore the role of the acceptor ligand in modulating key properties for possible DSPEC applications. For photoanode applications the key properties are (1) broad light absorption in the visible, (2) injection into conduction band states of TiO_2 or other oxides with appropriate acceptor potentials, and (3) sufficient potential as Ru^{3+} to drive water oxidation catalysis. Figure 12 addresses these issues by displaying how $E_{1/2}(Ru^{3+/2+*})$ and $E_{1/2}(Ru^{3+/2+})$ vary with the energy of the lowest energy MLCT absorption.

These results point to the interplay between these properties that is caused by variations in the lowest acceptor ligand. In the series $[Ru^{II}(bpy)_2(N{-}N)]^{2+}$, **1**−**9**, replacing bpy by N−N results in only slight increases in $E_{1/2}(Ru^{3+/2+})$ but with a shift of 121 nm (4.8×10^3 cm^{-1}) to lower energy for the lowest

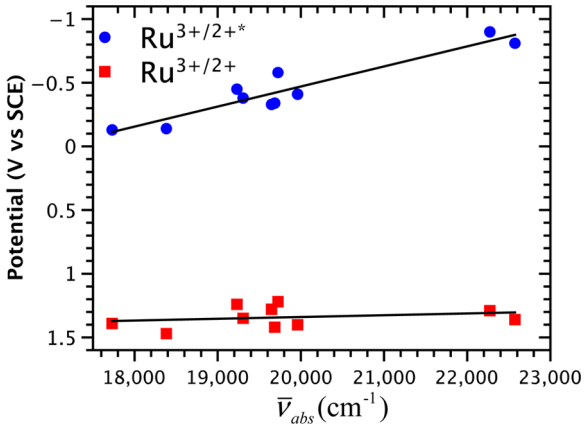

Figure 12. Variations in $E_{1/2}(Ru^{3+/2+})$ (red squares) and $E_{1/2}(Ru^{3+/2+*})$ (blue circles) with $\bar{\nu}_{abs}$ for the lowest energy MLCT λ_{max} in CH_3CN at room temperature.

energy MLCT absorption (Table 1). This is a desirable property with ligand variations shifting the low energy absorption edge to the red by lowering the π^* acceptor levels through increased conjugation or incorporation of heteroatoms in the N−N ligand.

Figure 12 shows how the two key redox potentials for photoanode applications, $E_{1/2}(Ru^{3+/2+})$ and $E_{1/2}(Ru^{3+/2+*})$, vary with $\bar{\nu}_{abs}$. Although the red-shifted absorption spectrum has a small effect on $E_{1/2}(Ru^{3+/2+})$ and water oxidation ability, it comes with a more positive $Ru^{3+/2+*}$ redox potential, limiting the ability of the excited state to act as a reducing agent. As an example, complex **9** is only slightly more oxidizing than $Ru(bpy)_3^{3+}$, 1.39 V compared to 1.29 V (vs SCE), and has a considerably red-shifted low energy MLCT absorption, 564 nm (22 200 cm^{-1}) compared to 449 nm (17 700 cm^{-1}) for $Ru(bpy)_3^{2+}$. However, this exchange of **L9** for bpy as the acceptor ligand increases $E_{1/2}(Ru^{3+/2+*})$ from −0.90 V to −0.13 V versus SCE, past the potential threshold for injection into TiO_2 with $E_{CB} \sim -0.34$ V (vs SCE) at pH 0 in water making **9** unable to undergo electron injection into TiO_2 following photoexcitation.[16,20,21]

SUMMARY AND CONCLUSIONS

We have described here the synthesis and characterization of polypyridyl complexes $[Ru(bpy)_2(N{-}N)]^{2+}$ (**1**−**9**) with N−N a bidentate polypyridyl ligand with low-lying π^* acceptor levels. Compared to $Ru(bpy)_3^{2+}$ as a reference, variations in N−N have a systematic effect on ground state and excited state redox potentials, absorption spectra, emission energies, and excited state lifetimes. The variations originate from the influence of increased delocalization or addition of heteroatoms on the π^* acceptor level(s) of N−N.

From the results of electrochemical measurements, variations in $E_{1/2}(Ru^{3+/2+})$ with N−N are relatively small and due to stabilization of Ru(II) by $d\pi-\pi^*$ backbonding. By contrast, there are significant variations in $E_{1/2}(Ru^{2+/+})$ with reduction occurring at the N−N ligand. Through the series, the lowest energy MLCT absorption is red-shifted relative to $Ru(bpy)_3^{2+}$ (λ_{max} = 449 nm) reaching λ_{max} = 564 nm for complex **9** with the band assignments in agreement with the results of TD-DFT calculations. Emission energies decrease from complex **1** (λ_{max} = 650 nm) to complex **9** (λ_{max} = 885 nm), relative to $Ru(bpy)_3^{2+*}$ (λ_{max} = 620 nm), with excited state lifetimes varying with emission energy in qualitative agreement with the energy gap law.

The results of Franck−Condon analyses of emission spectral profiles were used to calculate ΔG_{ES}, the free energy of the excited state above the ground state, and from ΔG_{ES}, redox potentials for the excited state couples $Ru^{3+/2+*}$ and $Ru^{2+*/+}$ were also calculated. ΔG_{ES} decreases through the series from **1** to **9** as a result of the decreasing energy of the π^* acceptor level(s) in N−N from **1** to **9**. $E_{1/2}(Ru^{2+*/+})$ for the metal-centered couple, $[Ru^{III}(bpy)_2(N{-}N^{\bullet-})]^{2+*}/[Ru^{II}(bpy)_2(N{-}N^{\bullet-})]^{+}$, is relatively unaffected by variations in N−N while $E_{1/2}(Ru^{3+/2+*})$ for the ligand-centered couple $[Ru^{III}(bpy)_2(N{-}N)]^{3+}/[Ru^{III}(bpy)_2(N{-}N^{\bullet-})]^{2+*}$ varies with $E_{1/2}(Ru^{2+/+})$. Comparisons in the series show that, with variations in the acceptor ligand, red-shifts in light absorption leave the oxidizing strength of Ru(III) relatively unaffected but increase $E_{1/2}(Ru^{3+/2+*})$ potentials past the threshold for injection into TiO_2.

dx.doi.org/10.1021/ic500408j | Inorg. Chem. 2014, 53, 5637−5646

■ ASSOCIATED CONTENT

Supporting Information

Table of emission spectral fitting parameters, UV−visible spectra, crystallographic data, calculation results, and experimental details. Crystallographic data in CIF format. This material is available free of charge via the Internet at http://pubs.acs.org

■ AUTHOR INFORMATION

Corresponding Author

*E-mail: tjmeyer@unc.edu.

Notes

The authors declare no competing financial interest.

■ ACKNOWLEDGMENTS

This work was primarily supported by the UNC Energy Frontier Research Center "Center for Solar Fuels", an Energy Frontier Research Center funded by the U.S. Department of Energy, Office of Science, Office of Basic Energy Sciences (DOE BES) under Award DE-SC0001011, supporting M.R.N., J.J.C., S.K., and M.K.B. We acknowledge support for D.L.A. from a fellowship from the Department of Energy Office of Science Graduate Fellowship Program (DOE SCGF), made possible by the American Recovery and Reinvestment Act of 2009, administered by ORISE-ORAU under Contract DE-AC05-06OR23100. C.R.K.G. acknowledges support from the UVA EFRC "Center for Catalytic Hydrocarbon Functionalization", an EFRC funded by DOE BES under Award DE-SC0001298. We also acknowledge Ken Hanson for the photophysical measurements of the compounds.

■ REFERENCES

(1) Hagfeldt, A.; Boschloo, G.; Sun, L.; Kloo, L.; Pettersson, H. *Chem. Rev.* **2010**, *110*, 6595.
(2) Song, W.; Chen, Z.; Glasson, C. R.; Hanson, K.; Lou, H.; Norris, M. R.; Ashford, D. L.; Concepcion, J. J.; Brennaman, M. K.; Meyer, T. J. *ChemPhysChem* **2012**, *13*, 2882.
(3) Lewis, N. S.; Nocera, D. G. *Proc. Natl. Acad. Sci. U.S.A.* **2006**, *103*, 15729.
(4) Concepcion, J. J.; Jurss, J. W.; Brennaman, M. K.; Hoertz, P. G.; Patrocinio, A. O. T.; Murakami Iha, N. Y.; Templeton, J. L.; Meyer, T. J. *Acc. Chem. Res.* **2009**, *42*, 1954.
(5) Eisenberg, R.; Gray, H. B. *Inorg. Chem.* **2008**, *47*, 1697.
(6) Fujishima, A.; Honda, K. *Nature* **1972**, *238*, 37.
(7) Wasielewski, M. R. *Chem. Rev.* **1992**, *92*, 435.
(8) Blankenship, R. E.; Tiede, D. M.; Barber, J.; Brudvig, G. W.; Fleming, G.; Ghirardi, M.; Gunner, M. R.; Junge, W.; Kramer, D. M.; Melis, A.; Moore, T. A.; Moser, C. C.; Nocera, D. G.; Nozik, A. J.; Ort, D. R.; Parson, W. W.; Prince, R. C.; Sayre, R. T. *Science* **2011**, *332*, 805.
(9) Khan, S. U. M.; Al-Shahry, M.; Ingler, W. B., Jr. *Science* **2002**, *297*, 2243.
(10) Bard, A. J.; Fox, M. A. *Acc. Chem. Res.* **1995**, *28*, 141.
(11) Meyer, T. J. *Acc. Chem. Res.* **1989**, *22*, 163.
(12) Hupp, J. T.; Neyhart, G. A.; Meyer, T. J.; Kober, E. M. *J. Phys. Chem.* **1992**, *96*, 10820.
(13) Hurst, J. K. *Science* **2010**, *328*, 315.
(14) Alstrum-Acevedo, J. H.; Brennaman, M. K.; Meyer, T. J. *Inorg. Chem.* **2005**, *44*, 6802.
(15) Treadway, J. A.; Moss, J. A.; Meyer, T. J. *Inorg. Chem.* **1999**, *38*, 4386.
(16) Swierk, J. R.; Mallouk, T. E. *Chem. Soc. Rev.* **2013**, *42*, 2357.
(17) Balzani, V.; Credi, A.; Venturi, M. *ChemSusChem* **2008**, *1*, 26.
(18) Gust, D.; Moore, T. A.; Moore, A. L. *Acc. Chem. Res.* **2009**, *42*, 1890.
(19) Wasielewski, M. R. *Acc. Chem. Res.* **2009**, *42*, 1910.
(20) Gratzel, M. *Nature* **2001**, *414*, 338.
(21) O'Regan, B.; Graetzel, M. *Nature* **1991**, *353*, 737.
(22) Green, A. N. M.; Palomares, E.; Haque, S. A.; Kroon, J. M.; Durrant, J. R. *J. Phys. Chem. B* **2005**, *109*, 12525.
(23) Vinodgopal, K.; Bedja, I.; Kamat, P. V. *Chem. Mater.* **1996**, *8*, 2180.
(24) Zheng, H.; Tachibana, Y.; Kalantar-zadeh, K. *Langmuir* **2010**, *26*, 19148.
(25) Sadek, A. Z.; Zheng, H.; Breedon, M.; Bansal, V.; Bhargava, S. K.; Latham, K.; Zhu, J.; Yu, L.; Hu, Z.; Spizzirri, P. G.; Wlodarski, W.; Kalantar-Zadeh, K. *Langmuir* **2009**, *25*, 9545.
(26) Kay, A.; Graetzel, M. *J. Phys. Chem.* **1993**, *97*, 6272.
(27) Gratzel, M. *Acc. Chem. Res.* **2009**, *42*, 1788.
(28) Ardo, S.; Meyer, G. J. *Chem. Soc. Rev.* **2009**, *38*, 115.
(29) Kaerkaes, M. D.; Johnston, E. V.; Verho, O.; Aakermark, B. *Acc. Chem. Res.* **2014**, *47*, 100.
(30) Frischmann, P. D.; Mahata, K.; Wuerthner, F. *Chem. Soc. Rev.* **2013**, *42*, 1847.
(31) Zong, R.; Thummel, R. P. *J. Am. Chem. Soc.* **2005**, *127*, 12802.
(32) Tseng, H.-W.; Zong, R.; Muckerman, J. T.; Thummel, R. *Inorg. Chem.* **2008**, *47*, 11763.
(33) Hanson, K.; Brennaman, M. K.; Ito, A.; Luo, H.; Song, W.; Parker, K. A.; Ghosh, R.; Norris, M. R.; Glasson, C. R. K.; Concepcion, J. J.; Lopez, R.; Meyer, T. J. *J. Phys. Chem. C* **2012**, *116*, 14837.
(34) Hanson, K.; Brennaman, M. K.; Luo, H.; Glasson, C. R. K.; Concepcion, J. J.; Song, W.; Meyer, T. J. *ACS Appl. Mater. Interfaces* **2012**, *4*, 1462.
(35) Brennaman, M. K.; Patrocinio, A. O. T.; Song, W.-J.; Jurss, J. W.; Concepcion, J. J.; Hoertz, P. G.; Traub, M. C.; Murakami Iha, N. Y.; Meyer, T. J. *ChemSusChem* **2011**, *4*, 216.
(36) Anderson, P. A.; Strouse, G. F.; Treadway, J. A.; Keene, F. R.; Meyer, T. J. *Inorg. Chem.* **1994**, *33*, 3863.
(37) Thompson, D. W.; Ito, A.; Meyer, T. J. *Pure Appl. Chem.* **2013**, *85*, 1257.
(38) Anderson, P. A.; Keene, F. R.; Meyer, T. J.; Moss, J. A.; Strouse, G. F.; Treadway, J. A. *J. Chem. Soc., Dalton Trans.* **2002**, 3820.
(39) Lever, A. B. P. *Inorg. Chem.* **1990**, *29*, 1271.
(40) Kalyanasundaram, K. *Coord. Chem. Rev.* **1982**, *46*, 159.
(41) Juris, A.; Balzani, V.; Barigelletti, F.; Campagna, S.; Belser, P.; Von Zelewsky, A. *Coord. Chem. Rev.* **1988**, *84*, 85.
(42) Caspar, J. V.; Meyer, T. J. *Inorg. Chem.* **1983**, *22*, 2444.
(43) Ashford, D. L.; Stewart, D. J.; Glasson, C. R.; Binstead, R. A.; Harrison, D. P.; Norris, M. R.; Concepcion, J. J.; Fang, Z.; Templeton, J. L.; Meyer, T. J. *Inorg. Chem.* **2012**, *51*, 6428.
(44) Ashford, D. L.; Song, W.; Concepcion, J. J.; Glasson, C. R.; Brennaman, M. K.; Norris, M. R.; Fang, Z.; Templeton, J. L.; Meyer, T. J. *J. Am. Chem. Soc.* **2012**, *134*, 19189.
(45) Hanson, K.; Torelli, D. A.; Vannucci, A. K.; Brennaman, M. K.; Luo, H.; Alibabaei, L.; Song, W.; Ashford, D. L.; Norris, M. R.; Glasson, C. R. K.; Concepcion, J. J.; Meyer, T. J. *Angew. Chem., Int. Ed.* **2012**, *51*, 12782.
(46) Norris, M. R.; Concepcion, J. J.; Harrison, D. P.; Ashford, D. L.; Fang, Z.; Binstead, R. A.; Templeton, J. L.; Meyer, T. J. *J. Am. Chem. Soc.* **2013**, *135*, 2080.
(47) Song, W.; Glasson, C. R. K.; Luo, H.; Hanson, K.; Brennaman, M. K.; Concepcion, J. J.; Meyer, T. J. *J. Phys. Chem. Lett.* **2011**, *2*, 1808.
(48) Concepcion, J. J.; Jurss, J. W.; Hoertz, P. G.; Meyer, T. J. *Angew. Chem., Int. Ed.* **2009**, *48*, 9473.
(49) Alibabaei, L.; Brennaman, K. M.; Norris, M. R.; Kalanyan, B.; Song, W.; Losego, M. D.; Concepcion, J. J.; Binstead, R. A.; Parsons, G. N.; Meyer, T. J. *Proc. Natl. Acad. Sci. U.S.A.* **2013**, *110*, 20008.
(50) Norris, M. R.; Concepcion, J. J.; Fang, Z.; Templeton, J. L.; Meyer, T. J. *Angew. Chem., Int. Ed.* **2013**, *52*, 13580.
(51) Cordeiro, A.; Shaw, J.; O'Brien, J.; Blanco, F.; Rozas, I. *Eur. J. Org. Chem.* **2011**, 1504.
(52) Norman, M. H.; Zhu, J.; Fotsch, C.; Bo, Y.; Chen, N.; Chakrabarti, P.; Doherty, E. M.; Gavva, N. R.; Nishimura, N.; Nixey,

T.; Ognyanov, V. I.; Rzasa, R. M.; Stec, M.; Surapaneni, S.; Tamir, R.; Viswanadhan, V. N.; Treanor, J. J. S. *J. Med. Chem.* **2007**, *50*, 3497.
(53) Sharma, K. S.; Kumari, S.; Singh, R. P. *Synthesis* **1981**, 316.
(54) Jung, D.-i.; Song, J.-h.; Kim, Y.-h.; Lee, D.-h.; Lee, Y.-g.; Park, Y.-m.; Choi, S.-k.; Hahn, J.-t. *Bull. Korean Chem. Soc.* **2007**, *28*, 1877.
(55) Zhao, Q.; Liu, S.; Shi, M.; Wang, C.; Yu, M.; Li, L.; Li, F.; Yi, T.; Huang, C. *Inorg. Chem.* **2006**, *45*, 6152.
(56) Goswami, S.; Maity, A. C.; Fun, H.-K.; Chantrapromma, S. *Eur. J. Org. Chem.* **2009**, 1417.
(57) Norris, M. R.; Concepcion, J. J.; Glasson, C. R. K.; Fang, Z.; Lapides, A. M.; Ashford, D. L.; Templeton, J. L.; Meyer, T. J. *Inorg. Chem.* **2013**, *52*, 12492.
(58) Gu, J.; Chen, J.; Schmehl, R. H. *J. Am. Chem. Soc.* **2010**, *132*, 7338.
(59) Biner, M.; Buergi, H. B.; Ludi, A.; Roehr, C. *J. Am. Chem. Soc.* **1992**, *114*, 5197.
(60) Yam, V. W.-W.; Lee, V. W.-M.; Ke, F.; Siu, K.-W. M. *Inorg. Chem.* **1997**, *36*, 2124.
(61) Rillema, D. P.; Mack, K. B. *Inorg. Chem.* **1982**, *21*, 3849.
(62) Ackermann, M. N.; Interrante, L. V. *Inorg. Chem.* **1984**, *23*, 3904.
(63) Nagle, J. K.; Young, R. C.; Meyer, T. J. *Inorg. Chem.* **1977**, *16*, 3366.
(64) Caspar, J. V.; Kober, E. M.; Sullivan, B. P.; Meyer, T. J. *J. Am. Chem. Soc.* **1982**, *104*, 630.
(65) Caspar, J. V.; Meyer, T. J. *J. Am. Chem. Soc.* **1983**, *105*, 5583.
(66) Wacholtz, W. F.; Auerbach, R. A.; Schmehl, R. H. *Inorg. Chem.* **1986**, *25*, 227.
(67) Kapovsky, M.; Dares, C.; Dodsworth, E. S.; Begum, R. A.; Raco, V.; Lever, A. B. P. *Inorg. Chem.* **2012**, *52*, 169.
(68) Durham, B.; Caspar, J. V.; Nagle, J. K.; Meyer, T. J. *J. Am. Chem. Soc.* **1982**, *104*, 4803.
(69) Van Houten, J.; Watts, R. J. *J. Am. Chem. Soc.* **1976**, *98*, 4853.
(70) Van Houten, J.; Watts, R. J. *Inorg. Chem.* **1978**, *17*, 3381.
(71) Norrby, T.; Boerje, A.; Aakermark, B.; Hammarstroem, L.; Alsins, J.; Lashgari, K.; Norrestam, R.; Maartensson, J.; Stenhagen, G. *Inorg. Chem.* **1997**, *36*, 5850.
(72) Allen, G. H.; White, R. P.; Rillema, D. P.; Meyer, T. J. *J. Am. Chem. Soc.* **1984**, *106*, 2613.
(73) Hammarstroem, L.; Barigelletti, F.; Flamigni, L.; Indelli, M. T.; Armaroli, N.; Calogero, G.; Guardigli, M.; Sour, A.; Collin, J.-P.; Sauvage, J.-P. *J. Phys. Chem. A* **1997**, *101*, 9061.
(74) Heully, J.-L.; Alary, F.; Boggio-Pasqua, M. *J. Chem. Phys.* **2009**, *131*, 184308/1.
(75) Sun, Q.; Mosquera-Vazquez, S.; Lawson Daku, L. M.; Guenee, L.; Goodwin, H. A.; Vauthey, E.; Hauser, A. *J. Am. Chem. Soc.* **2013**, *135*, 13660.
(76) Abrahamsson, M.; Lundqvist, M. J.; Wolpher, H.; Johansson, O.; Eriksson, L.; Bergquist, J.; Rasmussen, T.; Becker, H.-C.; Hammarstroem, L.; Norrby, P.-O.; Akermark, B.; Persson, P. *Inorg. Chem.* **2008**, *47*, 3540.
(77) Damrauer, N. H.; Boussie, T. R.; Devenney, M.; McCusker, J. K. *J. Am. Chem. Soc.* **1997**, *119*, 8253.
(78) Li, J.; Djurovich, P. I.; Alleyne, B. D.; Yousufuddin, M.; Ho, N. N.; Thomas, J. C.; Peters, J. C.; Bau, R.; Thompson, M. E. *Inorg. Chem.* **2005**, *44*, 1713.
(79) Gorelsky, S. I.; Dodsworth, E. S.; Lever, A. B. P.; Vlcek, A. A. *Coord. Chem. Rev.* **1998**, *174*, 469.
(80) Kober, E. M.; Marshall, J. L.; Dressick, W. J.; Sullivan, B. P.; Caspar, J. V.; Meyer, T. J. *Inorg. Chem.* **1985**, *24*, 2755.
(81) Kestell, J. D.; Williams, Z. L.; Stultz, L. K.; Claude, J. P. *J. Phys. Chem. A* **2002**, *106*, 5768.
(82) Knight, T. E.; Goldstein, A. P.; Brennaman, M. K.; Cardolaccia, T.; Pandya, A.; DeSimone, J. M.; Meyer, T. J. *J. Phys. Chem. B* **2011**, *115*, 64.
(83) Nozaki, K.; Takamori, K.; Nakatsugawa, Y.; Ohno, T. *Inorg. Chem.* **2006**, *45*, 6161.
(84) Kim, H. B.; Kitamura, N.; Tazuke, S. *J. Phys. Chem.* **1990**, *94*, 7401.
(85) Ito, A.; Meyer, T. J. *Phys. Chem. Chem. Phys.* **2012**, *14*, 13731.
(86) Caspar, J. V.; Meyer, T. J. *J. Phys. Chem.* **1983**, *87*, 952.
(87) Dattelbaum, D. M.; Martin, R. L.; Schoonover, J. R.; Meyer, T. J. *J. Phys. Chem. A* **2004**, *108*, 3518.
(88) Yersin, H. *Top. Curr. Chem.* **2004**, *241*, 1.
(89) Vogler, L. M.; Jones, S. W.; Jensen, G. E.; Brewer, R. G.; Brewer, K. J. *Inorg. Chim. Acta* **1996**, *250*, 155.
(90) Dattelbaum, D. M.; Omberg, K. M.; Schoonover, J. R.; Martin, R. L.; Meyer, T. J. *Inorg. Chem.* **2002**, *41*, 6071.